Journal of Alloys and Compounds, 194 (1993) 189–197
JALCOM 7229

Solid-state amorphizing transformations: thermodynamics and kinetics*

R. B. Schwarz and J. B. Rubin
Center for Material Science,, Los Alamos National Laboratory, Los Alamos, NM 87545 (USA)

(Received June 1, 1992)

Abstract

Amorphous metallic alloys are thermodynamically metastable with respect to one or more crystalline phases. Forming an amorphous alloy by an isothermal solid-state transformation requires starting from a state of free energy higher than that of the amorphous phase and choosing a reaction path that prevents the system from reaching the crystalline state of lowest free energy. Much has been learned about solid-state amorphizing transformations from interdiffusion experiments in transition-metal thin-film multilayers. We review some of these experiments and discuss recent advances in our understanding of the thermodynamics and kinetics of the phenomenon.

1. Introduction

Amorphous metallic alloys are thermodynamically metastable with respect to one or more crystalline phases. The first synthesis of amorphous metallic alloys was reported by Buckel and Hilsh [1] who, in 1954, prepared amorphous metallic films by condensing elemental vapors onto cryogenically cooled substrata. The amorphous structure of the films was deduced from *in situ* electron diffraction measurements. These amorphous films crystallized, however, when heated to a few tens of kelvin. Because atomic bonding in metals is highly non-directional, three-dimensional amorphous aggregates of a single species, or of species of similar electronegativity, have a low resistance to crystallization. It was soon realized that pure metals such as copper and gold are almost impossible to prepare in the amorphous state unless the film also contains some impurities. The situation is quite different in a binary alloy, $A_{1-x}B_x$, between atom species A and B that have vastly different electronegativities. Here, the A–B bonds are stronger than either A–A or B–B bonds, providing resistance to short-range atomic rearrangement: such alloys, when in the amorphous state, usually have crystallization temperatures between 40% and 60% of the alloy's melting temperature, T_m.

Figure 1 is a composition *vs.* temperature diagram for a hypothetical binary A–B system. In equilibrium

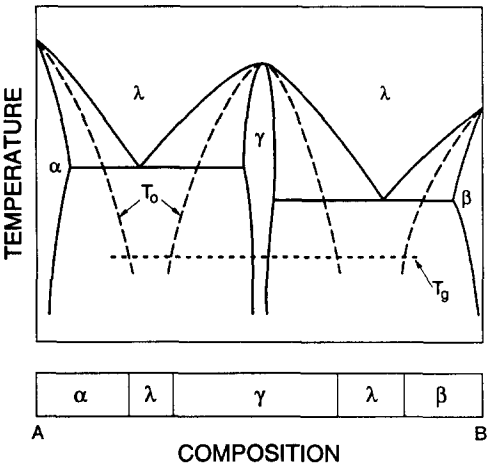

Fig. 1. Schematic phase diagram for a binary system with a negative enthalpy of mixing in the liquid state.

the system forms two solid solutions of limited solubilities, α and β, and a congruently melting compound γ. The T_0 curves are the loci of temperature–composition points where the free energies of phases α, β, and γ equal that of the liquid phase λ. In effect, the figure contains two phase diagrams: the solid curves define the equilibrium phase boundaries in the presence of solute partitioning, whereas the T_0 lines define the metastable boundaries when solute partitioning is suppressed. We see that in the latter case, the liquid phase in between the T_0 lines extends to very low temperatures. As the temperature of the liquid is decreased, however, its viscosity rapidly increases. When the viscosity reaches a value of 10^{13} P, corresponding approximately to one

*Paper presented at the Symposium on Solid State Amorphizing Transformations, TMS Fall Meeting, Cincinnati, OH, October 21–24, 1991.

atomic jump per atom per day, the undercooled liquid is considered to be a glass. This transition is a customary definition of the glass transition temperature, T_g.

Crystallization involving solute partitioning is difficult to suppress unless the melt is rapidly cooled. The best known methods for synthesizing amorphous metallic alloys are based on the rapid solidification (RS) of molten alloys [2] at cooling rates of 10^4 K s^{-1} or higher. Added to Fig. 1 is a hypothetical composition invariant glass transition temperature curve, T_g. From these considerations follow the two requirements for preparing a glass by the RS technique:

(a) *Thermodynamic requirement*: Existence of a metastable amorphous state (T_0 lines that cross the T_g curve at a temperature above that where the T_0 lines intersect each other).

(b) *Kinetic requirement*: A sufficiently high cooling rate to avoid partitionless crystallization of the melt in the regime $T_m > T > T_g$.

The bar graph at the bottom of Fig. 1 shows the homogeneity ranges of phases α, λ, γ, and β predicted by the intersection of the T_0 and T_g lines. This construction, however, assumes that in the absence of solute partitioning, phases α, β, and γ form as soon as the T_0 curves are crossed on cooling. In reality, formation of these phases by a partitionless nucleation and growth process requires a finite degree of undercooling. When such kinetic effects are included [3], the T_0 curves are displaced downwards in temperature, resulting in a narrowing of the composition ranges for the α, β, and γ phases and a widening of the two glass-forming regions, λ. For cooling rates of the order of 10^{12} K s^{-1}, typical of laser-quenching experiments [4] and for alloy formation by vapor condensation [5], the glass-forming regions widen to include all intermediate compositions, excluding only the narrow terminal solid-solution fields, α and β.

New methods for synthesizing amorphous metallic alloys have been developed recently that do not rely on the solidification of melts. Malik and Wallace [6] and Yeh *et al.* [7] reported that the isothermal reaction of certain crystalline intermetallics with hydrogen leads to the formation of amorphous hydrides. Similarly to equilibrium (thermodynamic) melting, the crystal-to-amorphous transformation starts at lattice defects such as grain boundaries [8]. In 1981, Hauser [9], and later Herd *et al.* [10] reported that certain transition metals can diffuse at low temperatures into amorphous semiconductors such as tellurium, selenium, and silicon, without causing the semiconductor to crystallize. In 1983, Schwarz and Johnson [11] reported the first example of two pure crystalline metals, lanthanum and gold, reacting isothermally to form a single-phase amorphous alloy.

Figure 2 illustrates the free energies of the phases α, β, and λ at a temperature $T < T_g$. The solid-state amorphizing reaction (SSAR) starts with a mechanical mixture of metals A and B. For an equimolar mixture the initial free energy is that of point 1. If the mixture is reacted at high temperatures, it would reach the crystalline state, 3, of lowest free energy. However, if the reaction is done at a temperature that is too low for the nucleation of phase γ, the system may then reach the metastable amorphous state, 2. The reaction rates between these states may be characterized, in a simplified manner, by reaction times τ, where the indices i, a, and x refer to the initial, amorphous, and crystalline states, respectively. The requirements for glass formation by a SSAR at the reaction temperature T_r are:

(a) *Thermodynamic requirement*: A large negative enthalpy of mixing between metals A and B to ensure the existence of a high-energy initial state at $T = T_r$.

(b) *Kinetic requirement*: A large difference between the diffusivities of A and B in the amorphous alloy AB to ensure:

$$\tau(\mathrm{i} \rightarrow \mathrm{a}) \ll \tau(\mathrm{i} \rightarrow \mathrm{x})$$

$$\tau(\mathrm{i} \rightarrow \mathrm{a}) \ll \tau(\mathrm{a} \rightarrow \mathrm{x})$$

$$\tau(\mathrm{i} \rightarrow \mathrm{a}) \simeq 10^5 \text{ s}$$

The kinetic requirements are expressed by inequalities between the characteristic reaction times, Fig. 3. The first two inequalities ensure that the amorphous alloy will be formed in preference to crystalline compound(s) of lower free energy and that, during its formation, the amorphous alloy will not crystallize. The last inequality is somewhat arbitrary and expresses the re-

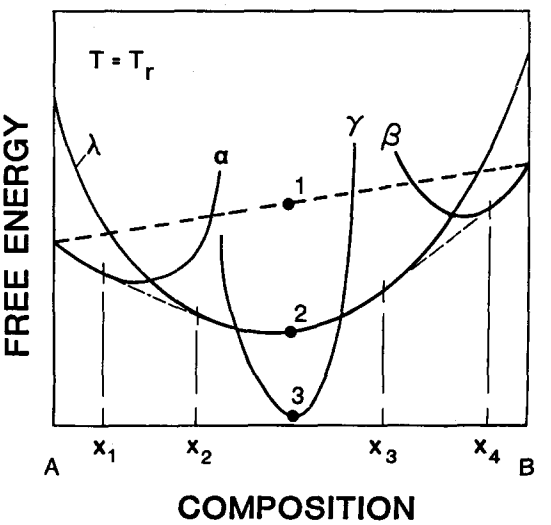

Fig. 2. Free-energy diagram for the phases in Fig. 1 at the temperature T_r. The common tangents to the free-energy curves of phases α, β, and λ determine the reaction products at T_r, which is too low to promote the nucleation and growth of the intermetallic phase λ.

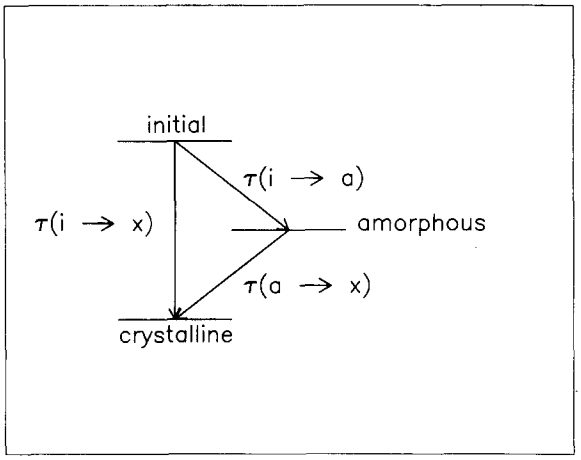

Fig. 3. Characteristic reaction times for the formation of amorphous and crystalline phases from an initial high-energy state.

quirement that the reaction be completed within a reasonable time. These inequalities are satisfied by a proper choice of the reaction temperature.

2. SSARs in thin films

Thin-film technology is ideal for studying SSARs because it allows us to prepare the initial state in a simple way. By condensing vapors of two pure metals onto a substrate kept near ambient temperature, the initial state can be prepared as a multilayer of alternating thin elemental films. Following deposition, the multilayer is annealed *in situ* at the temperature T_r while the SSAR is monitored by techniques such as X-ray diffraction or electrical resistance. We present examples of both measurements.

Figure 4 shows X-ray diffraction patterns [11] for a multilayer of gold and lanthanum films in the as-deposited condition, (d), and following thermal anneals at 70 °C for the indicated times. Curve (a) is for a multilayer rich in gold whereas curve (c) is for a multilayer rich in lanthanum. Curve (b) is for a multilayer of near equimolar composition. The gold–lanthanum system fulfills the two SSAR requirements stated earlier: (a) the enthalpy of mixing of Au and La in the liquid state is $\Delta H_m = -73$ kJ mol^{-1} [12]; and (b) gold is an anomalously fast diffuser in crystalline lanthanum. Presumably, it is also a fast diffuser in the amorphous alloy phase.

The SSAR in nickel–zirconium multilayers has been extensively studied [13–15]. The enthalpy of mixing of nickel and zirconium in the liquid state is $\Delta H_m = -49$ kJ mol^{-1} [12], which provides the thermodynamic driving force for the reaction. In addition, nickel and zirconium have vastly different diffusivities in each other and in the amorphous phase. Figure 5 shows the electrical resistance, R, of a stack of alternating thin films of

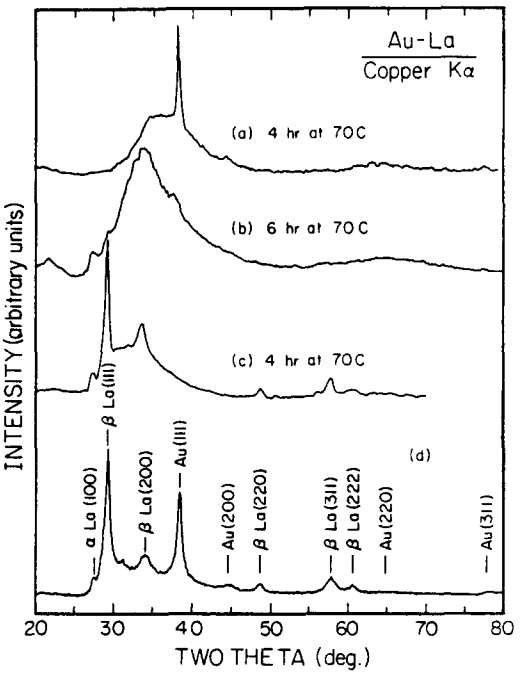

Fig. 4. X-ray scattered intensity as a function of scattering angle for gold–lanthanum multilayers. Curves (a), (b), and (c) are for annealed samples that are gold-rich, equiatomic, and lanthanum-rich, respectively. Curve (d) is for an unreacted (as-deposited) multilayer sample with a composition similar to that of curve (b).

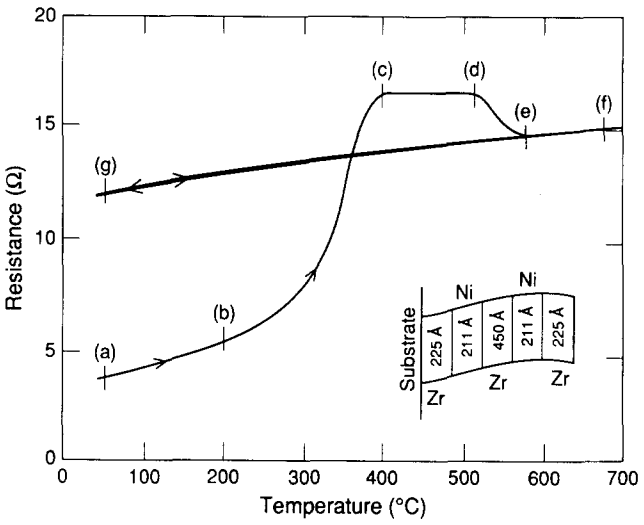

Fig. 5. Resistance of a multilayer system of nickel and zirconium thin films during the continuous heating and cooling at 10 K min^{-1}. The sample configuration is shown in the inset.

nickel and zirconium as a function of temperature. These data were obtained [16] during continuous heating from 300 to 1000 K, followed by cooling to 300 K, at the rate of 10 K min^{-1}. Figure 6 illustrates the structural changes occurring in the films during this thermal cycle, as deduced from X-ray diffraction measurements. The initial thickness of the films, indicated in the inset of Fig. 5, are those necessary to form an equimolar amor-

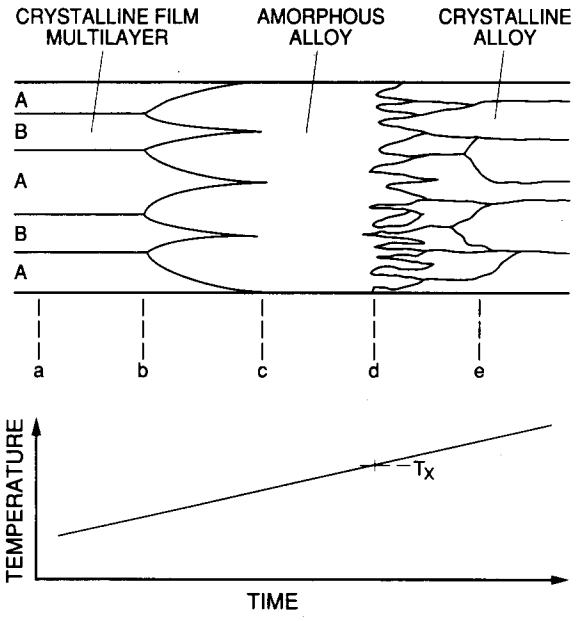

Fig. 6. Schematic of the structural changes occurring when the thin film multilayer in the inset of Fig. 5 is annealed at a constant heating rate. The letters (a)–(e) correspond to those in Fig. 5.

phous alloy. Letters have been added to both figures to indicate intermediate steps in the reaction. Between (a) and (b) the temperature is too low for interdiffusion and R increases nearly linearly with increasing temperature, as expected for pure crystalline metals. At (b), amorphous alloy begins to form at each of the Ni–Zr interfaces. Because the resistance of the amorphous NiZr alloy is higher than that of the initial pure nickel and zirconium, the resistance of the multilayer increases as the reaction proceeds. The SSAR ends at (c) when all the Ni and Zr have been consumed. The resistance is constant from (c) to (d), in agreement with the observation that the resistivity of amorphous alloys is largely temperature independent. At (d), a crystalline alloy phase nucleates in the amorphous alloy and the resistance decreases as long-range order develops. From (d) to (e), the resistance decreases as the transformation proceeds by a two-step crystallization [17] and the crystals grow in size. At (e), the alloy has reached the thermodynamically stable crystalline state that is unaffected by further temperature variations. For further cooling and heating cycles, (e)–(f)–(g), the resistivity of the crystalline alloy has the expected positive linear temperature dependence.

It is clear from Fig. 5 that the temperature T_b at which the amorphization commences must be significantly lower than the temperature T_d at which crystallization of the amorphous alloy begins. In our current understanding of the SSAR, we identify T_b as the temperature where nickel, the smaller and faster-diffusing atom, becomes mobile in the amorphous alloy formed at each of the Ni–Zr interfaces. This mobility is sufficient to enable nickel atoms to diffuse from the nickel film, across the amorphous alloy already formed, to reach the zirconium film and form additional amorphous phase. At T_d, zirconium also becomes mobile in the amorphous phase and this enables the alloy to crystallize. Thus, the temperature difference, T_d-T_b, is the *temperature window* for the SSAR. Certainly, this window depends on heating rate. In isothermal experiments, T_r is chosen near the lower end of this window. At the completion of the SSAR, the amorphous layer has a modulated composition that becomes homogeneous through further annealing.

Experience has shown that all binary systems where a SSAR has been observed [18, 19] obey the thermodynamic and kinetic conditions stated previously. Systems that obey these two conditions include alloys of an early transition metal (ETM), typically elements from groups IIIA, IVA, and VA, and a late transition metal (LTM), group VIIIA, or a noble metal. For these pairs of metals, the tracer diffusivity of the LTM in the crystalline ETM is several orders of magnitude larger than the self-diffusivity of either element [20, 21]. This asymmetry in diffusivities has been correlated with the difference in atomic sizes [22]. Turnbull [23] proposed that the asymmetry in diffusivities occurs because some of the LTM atoms dissolve interstitially in the lattice of the ETM. The dependence of diffusivities on atomic size found in crystals appears also in the amorphous state. Hahn and co-workers [24, 25] have shown that the tracer diffusivity of transition metals in amorphous $Ni_{50}Zr_{50}$ is a strong but smooth function of their atomic size. For example, in amorphous Ni–Zr, the diffusivity of nickel exceeds that of titanium by more than three orders of magnitude. These data suggest an even larger difference in diffusivities for nickel and zirconium [26]. Hahn *et al.* suggest that an interstitial diffusion mechanism similar to that occurring in crystalline ETMs operates in the amorphous Ni–Zr alloy.

3. Nucleation of the SSAR

In the first SSAR experiments on the Au–La system, Schwarz and Johnson [11] deposited an *amorphous* AuLa film between the polycrystalline Au and La films. Their initial thought was that such a film was necessary to provide amorphous nuclei for the initiation of the SSAR. They soon discovered, however, that the SSAR proceeded equally well without the intermediate amorphous film. The interface between polycrystalline Au and La films seems to contain a large density of defects that facilitates the nucleation of the amorphous phase. Soon after, Schroeder *et al.* [27] did the first cross-sectional transmission electron microscopy (TEM) ob-

servations of a SSAR in progress. They observed that in Co–Zr thin film multilayers the amorphous film has a uniform thickness from the start of the reaction, again indicating that the interfaces contain a large density of (heterogeneous) nucleation centers for the amorphous phase.

Data obtained from a large number of experiments in thin films suggest that the growth of the amorphous phase by a SSAR is analogous to equilibrium melting, proceeding by classical nucleation and growth [8]. Vredenberg *et al.* [28] reported first that the SSAR does not occur in diffusion couples of polycrystalline Ni deposited onto single-crystal Zr. The SSAR proceeded normally, however, if the films were ion irradiated before annealing; the intermixing produced by the irradiation is sufficient to nucleate the amorphous phase, enabling the SSAR to proceed. A diffusion couple of polycrystalline Ni on recrystallized Zr also failed to react when isothermally annealed [29]. In contrast, a diffusion couple of polycrystalline Zr deposited onto single crystal Ni produces an amorphous phase by the SSAR [30]. In a third study, Ehrhart *et al.* [31] annealed bilayer couples formed by: (a) polycrystalline Ni and single-crystal Zr; (b) amorphous NiZr and single-crystal Zr; and (c) single-crystal $Ni_{0.01}Zr_{0.99}$ and single-crystal Zr. A SSAR was observed only in case (b) which had an initial amorphous layer at the interface. These results have been interpreted as meaning that the SSAR requires the presence of Zr grain boundaries as nucleation sites for the amorphous phase. The presence of Zr grain boundaries, however, seems to be a sufficient, but not a necessary condition, as we discuss next.

Figure 7 shows the (metastable) zirconium-rich end of the Ni–Zr phase diagram. We have omitted the invariant lines associated with the formation of crystalline intermetallic compounds. The phase fields for $T > 850$ °C are from the assessed equilibrium phase diagram [32]. The dashed curves indicate the extrapolated $\alpha+\beta$ phase field. The metastable phase diagram predicts an invariant reaction $\beta \rightarrow \lambda + \alpha$ at about 820 °C. The horizontal dash–dot line represents the SSAR temperature, $T_r = 280$ °C. Figure 8 shows the free energy curves for the amorphous phase, λ, and the b.c.c. Zr phase, β, calculated at T_r using a CALPHAD thermodynamic model. For these calculations we used the lattice stabilities from Kaufman and Bernstein [33] and the excess free-energy parameters given by Saunders and Miodownik [34, 35]. These authors also predict the free energy of the hcp α-Zr phase but this prediction is reliable only for very low nickel concentrations. This is so because their thermodynamic modeling is based on equilibrium data that has extremely low Ni solubility (less than 0.6 at.%). The limited solubility of Ni in α-Zr suggests that the α-Zr(Ni) phase is characterized by a large *positive* enthalpy of mixing. Whereas the chemical and entropic contributions to the enthalpy of mixing in α-Zr are negative, the total mixing enthalpy of α-Zr(Ni) is positive apparently because of the large strain energy that must be supplied to substitute a Ni atom in the α-Zr lattice, which Highmore estimates to be 1.6 eV [36]. With this in mind, we have plotted schematically the free-energy curve for α-Zr.

Let us assume that a Ni–Zr thin film multilayer with clean interfaces (no amorphous or crystalline interlayer) is annealed at T_r for a long time. The terminal solubility of Ni in Zr is given by the common tangent, shown

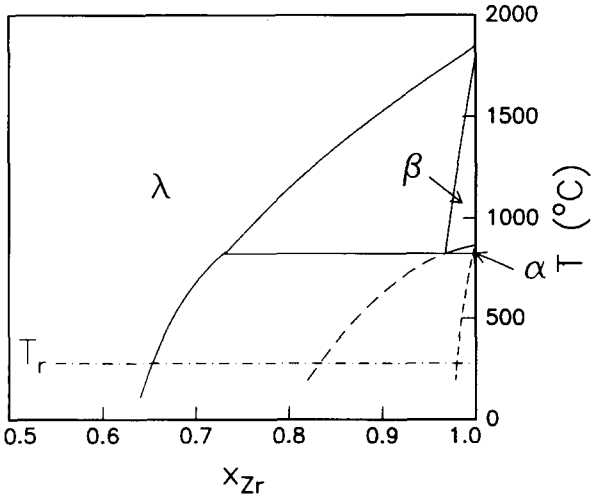

Fig. 7. Metastable zirconium-rich end of the Ni–Zr phase diagram. The dashed curves are extrapolations of the boundaries for the $(\alpha+\beta)$ phase field. The horizontal dash–dot line denotes the temperature for the SSAR.

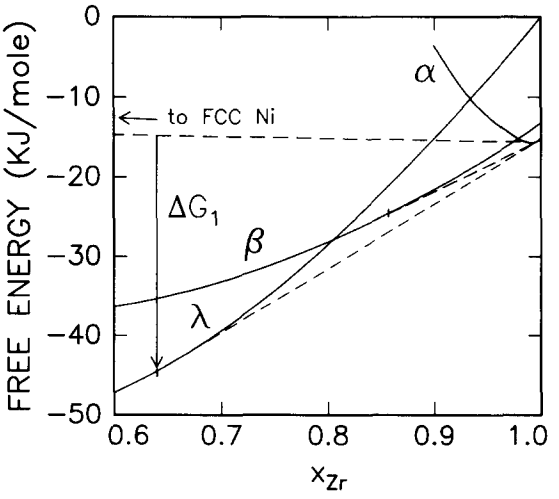

Fig. 8. Free-energy curves for the h.c.p. (α) and b.c.c. (β) Zr-rich solid solutions, and the amorphous phase, λ. The dashed lines are the common tangents between α-Zr and f.c.c. Ni, α-Zr and β-Zr, and α-Zr and λ phase. ΔG_1 is the thermodynamic driving force for the formation of λ-phase from a mixture of Ni and α-Zr.

as a dashed line in Fig. 8, between the α-Zr curve and the f.c.c.-Ni free-energy curve. We see from this construction that in the absence of an amorphous or crystalline interlayer, the terminal solubility of Ni in Zr is extremely small. Although there is a thermodynamic driving force for the formation of an amorphous phase of composition close to $Ni_{36}Zr_{64}$, the nucleation of this phase is unlikely because it requires a very large compositional fluctuation. The diagram also shows a thermodynamic driving force for the formation of the β phase. Experience has shown that when the formation of equilibrium phases is hindered, one or more metastable transition phases nucleate instead. These transition phases grow and later facilitate the formation of more stable phases. In the present case it is possible that the β phase, with a composition close to $Ni_{15}Zr_{85}$, forms before the amorphous phase since it requires a much smaller composition fluctuation. There is an additional reason why the formation of β nuclei should be favored over the formation of amorphous (λ) nuclei. In the absence of heteronucleants, the amorphous nucleus must form by homogeneous nucleation, requiring an activation energy proportional to $(\sigma^3/\Delta G_1^2)$, where σ is the amorphous-crystal interfacial energy and ΔG_1 is the thermodynamic driving force (Fig. 8). In contrast, β nuclei could form within the α-Zr phase by a simple Burgers shear transformation [37]; because the β-nuclei formed in this way are coherent with the parent α-Zr phase, the Burgers transformation requires a much lower activation energy [38]. The situation is analogous to the formation of Guinier–Preston zones in supersaturated Al(Cu) solid solutions. These consist of coherent plate-like clusters of copper atoms on {100} aluminum planes, each plate being about 10 nm in diameter and as thin as a monolayer. In the present model, thin plates of {100} β-$Ni_{15}Zr_{85}$ would form on {00.2} planes of α-Zr. Once these precursor b.c.c. nuclei grow and reach a critical size, the λ phase could form since now its nucleation requires a much smaller compositional fluctuation.

The b.c.c. phase could nucleate at dislocations, both isolated and in arrays, and at sites not resolved by TEM (*e.g.* at vacancy clusters) [38]. Because these sites are most likely present in polycrystals as well as in single crystals, why then is the SSAR suppressed when polycrystalline Ni is deposited onto an α-Zr single crystal? The present model explains this phenomenon by the large strains that must be accommodated to allow for the h.c.p. $\rightarrow$ b.c.c. transformation. Although transformation shear strains are generally released by the generation of twins in the transformed phase [39], it is clear that the transformation strains would be easily relieved in fine-grained polycrystalline films, with more difficulty in large-grained materials, and perhaps not at all in single crystals. This would make the nucleation of the b.c.c. phase in single-crystal Zr impossible, inhibiting the SSAR.

In virtually all of the ETM–LTM systems known to amorphize *via* a SSAR, the ETM (Zr, T, Y, La, Hf) has a hexagonal-to-cubic transformation at a temperature significantly lower than T_m. This means that the difference in free energy between the two structures at T_r (typically 300 °C) is small. Thus, the b.c.c. phase should be thermodynamically accessible. An interesting experiment that would test the present model for the initiation of the SSAR would be to anneal isothermally a diffusion couple composed of polycrystalline Ni and single-crystal Nb. Because (1) polycrystalline Nb is known to form amorphous alloys by a SSAR with polycrystalline Cu, Ni, etc, and (2) Nb does not undergo any allotropic phase changes, and is cubic at all temperatures, we expect that the SSAR would also proceed at the interface of a single crystal of Nb and a polycrystalline Ni film.

4. SSARs in the absence of heteronucleation

The SSAR experiments in thin film diffusion couples, and of hydrogen diffusion into crystalline intermetallics, is allowing us a detailed look into the more general problem of melting.

Johnson [40] remarks that the classical nucleation theory developed by Becker and Doring and later by Turnbull [41] for the case of crystal nucleation from undercooled melts parallels that of melting in the sense that the interface that separates the ordered and disordered phases is the same whether one superheats the ordered phase or undercools the disordered phase. This symmetry is not apparent in nature because, experience has shown, it is much easier to undercool a liquid than to superheat a crystal. The asymmetry, however, is satisfactorily explained by the influence of heteronucleants. For the melting of crystals, lattice defects and free surfaces provide a copious density of heteronucleants that are rather difficult to suppress. The experiments of Dages *et al.* [42] where both types of heteronucleants were removed from small silver single crystals coated by a thin epitaxial overlay of gold, show that crystals can indeed be superheated, although by less than 10 K in these experiments. Crystal nucleation in undercooled melts, however, is relatively easy to suppress. For example, pure metals have been undercooled by several hundred kelvin by emulsifying molten drops in an immiscible liquid of lower melting temperature [43]. Alloy melts are even easier to undercool. For example, gram-size liquid samples of $Ni_{40}Pd_{40}P_{20}$ can be slowly undercooled to below the glass-transition temperature once oxide inclusions and other heteronucleants have been disolved in a flux [44].

If heteronucleants are removed from both undercooled liquids and superheated crystals, so as to frustrate any phase transformation involving solute partitioning then the question arises as to what are the absolute limits to which melts can be undercooled and crystals superheated? To answer this question we must look at the evolution of the thermodynamic state functions as the temperature deviates from the thermodynamic melting temperature, T_m.

That the entropy of an undercooled liquid decreases as T is decreased, and approaches the entropy of the crystal at a temperature close to T_g, has been known for nearly 60 years [45]. Figure 9 shows the entropy of liquid and crystalline ortho-terphenyl, $C_{18}H_{14}$ [46]. Kauzmann [47] analyzed the entropy data for organic liquids available at that time, and argued that an *apparent paradox* existed in that if the glass transition were not to occur, then on further cooling the entropy of the undercooled liquid would continue to decrease, becoming lower than that of the crystal of the same composition. He answered this paradox (thus his use of the word *apparent*) by discussing that, in agreement with the third law of thermodynamics, the configurational entropy of the *ideal* glass is zero. This, by itself a surprising result, had been previously proposed by Pauling and Tolman [48]. The bending of the $S_L(T)$ curve for the real glass in Fig. 9 at T slightly below T_g occurs simply because at that temperature the undercooled liquid has lost most of its configurational entropy and has nothing else to give on further cooling.

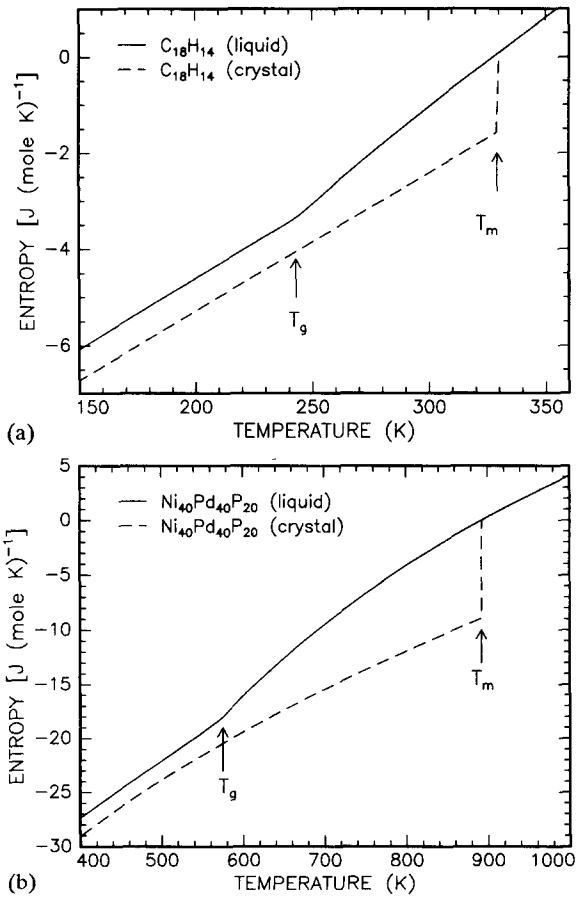

Fig. 9. (a) Entropy of liquid and crystalline ortho-terphenyl ($C_{18}H_{14}$) as a function of temperature obtained by integrating the $c_p(T)$ data of ref. 46; (b) Entropy of liquid and crystalline $Ni_{40}Pd_{40}P_{20}$ as a function of temperature obtained by integrating the $c_p(T)$ data of ref. 44.

The authors know of no example where on undercooling the melt the $S_L(T)$ curve crosses the $S_x(T)$ curve. For those few metallic alloys where $c_p(T)$ data are available for both the undercooled liquid and the crystal states in the regime $T_g < T < T_m$ [44], a simple integration [49] shows that at temperatures slightly below the observed T_g, S_L exceeds S_x by about $\Delta S \approx 0.25 \Delta H_m/T_m$. Although by lowering the cooling rate to infinitesimal values we should obtain somewhat lower T_g and ΔS values (the glass approaches the *ideal* glass), it is still unlikely that the $S_L(T)$ and $S_x(T)$ curves would ever cross; this is because the *ideal* glass has a higher vibrational entropy than the crystal because of its lower density. For such crossing to become possible, highly unusual circumstances would have to occur such as: (a) the vibrational entropy of the crystal exceeding the vibrational entropy of the glass; and/or (b) chemical ordering in the liquid exceeding that in the crystal [50]. Possibility (a) would occur, for example, if Zener- or Snoek-type defects were excited at $T = T_g$ in the crystal but not in the undercooled liquid.

The Kauzmann temperature, T_K, is defined as the temperature at which the *extrapolation* of the $S_L(T)$ curve crosses the $S_x(T)$ curve. Fecht *et al.* [51] have identified T_g with T_K and have proposed a polymorphous phase diagram for Zr-rich Ni–Zr alloys, Fig. 10. The T_0 curve, corresponding to $\Delta G = 0$, is rather well defined for $T > 1233$ K (above the β-Zr–$NiZr_2$ eutectic tem-

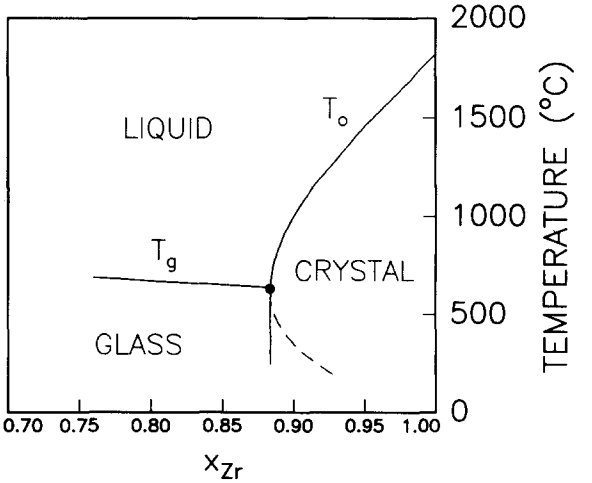

Fig. 10. Polymorphous phase diagram for Zr-rich Ni–Zr alloys, after ref. 51.

perature). Below 1233 K, the T_0 curve was calculated by composition–temperature polynomials (CALPHAD modeling) describing the free energies of the equilibrium liquid and crystal phases, which were extrapolated to $T_K \approx 600$ K. Because of the extent of the extrapolation, the shape of the T_0 curve near 600 K is highly unreliable, as demonstrated by Schwarz *et al.* [52]. Of importance, however, is the hypothetical crossing of the T_0 and T_K curves. At this critical point, $\Delta G = 0$, $\Delta S = 0$, and consequently, $\Delta H = 0$. Because the crystal–liquid surface tension, σ, is proportional to either ΔH [53] or ΔS [54], σ would also vanish at that point. Fecht *et al.* propose that at the triple point (coexistence of the crystal, liquid, and amorphous phases) the glass formation is isoentropic, isoenthalpic, and occurs catastrophically ($\sigma = 0$).

There are as yet no experimental data to support the polymorphic phase diagram in Fig. 10, and the existence of a triple point. At the composition of the triple point, an amorphous Ni–Zr alloy would crystallize with zero enthalpy of crystallization, which seems contrary to experimental evidence [55]. The scarcity of c_p data for liquids undercooled to $T \approx T_g$ makes it difficult to evaluate quantitatively the polymorphic model. The available data, however, suggest that neither ΔS nor ΔH become zero as T approaches T_g. For example, integrating the $c_p(T)$ data of Kui and Turnbull for $Ni_{40}Pd_{40}P_{20}$ [44], Schwarz and Nash [49] find that at $T_g = 580$ K, $\Delta S \simeq 0.25\ \Delta S_m$ and $\Delta H \simeq 0.30\ \Delta H_m$. This composition is, however, close to a ternary eutectic and could be quite different from that at the triple point. It appears that the simplest method to test the polymorphic phase diagram is to measure the enthalpy of crystallization in amorphous $Ni_{1-x}Zr_x$ thin films prepared by the condensation of vapor. For this synthesis technique, the homogeneity range of the amorphous phase is continuous from $0.10 < x < 0.90$ [3] and thus should include the composition of the critical point.

Fecht and Johnson [56] have proposed that for pure metals the $S_L(T)$ and $S_x(T)$ curves cross not only at T_K (below T_m), but also above T_m. In analogy to the proposed catastrophic crystallization of an undercooled melt, the superheated crystal should also melt catastrophically at a temperature $T_i^S > T_m$, where the $S_L(T)$ and $S_x(T)$ curves supposedly cross again. This second crossing is attributed to an increase in the crystal specific heat due to an increase in the density of vacancies. A lambda-shaped anomaly in the specific heat of $Fe_2ErH_{3.4}$ was taken by Fecht *et al.* [57] as evidence for the upper isoentropic transition. More recent experiments, however, suggest that the anomaly may have been an experimental artifact [58].

In conclusion, the existence of a composition–temperature phase diagram that gives a thermodynamic (polymorphic) boundary between the crystal, liquid, and glass phases is still an unresolved question.

Acknowledgment

This work was supported by the U.S. Department of Energy, Office of Basic Energy Sciences.

References

1 W. Buckel and R. Hilsch, *Z. Phys., 138* (1954) 109.
2 P. Duwez, R. H. Willens and W. Klement, Jr., *J. Appl. Phys., 31* (1960) 1136.
3 P. Nash and R. B. Schwarz, *Acta Metall., 36* (1988) 3047.
4 C. J. Lin and F. Spaepen, *Acta Metall., 34* (1986) 1367.
5 J. B. Rubin and R. B. Schwarz, *Mater. Res. Symp. Proc., 230* (1992) 21.
6 S. K. Malik and W. E. Wallace, *Solid-State Commun., 24* (1988) 283.
7 X. L. Yeh, K. Samwer and W. L. Johnson, *Appl. Phys. Lett., 42* (1983) 242.
8 R. W. Cahn and W. L. Johnson, *J. Mater. Res., 1* (1986) 724.
9 J. J. Hauser, *J. Phys. (Paris) Colloq., 42* (1981) C9-943.
10 S. R. Herd, K. N. Tu and K. Y. Ahn, *Appl. Phys. Lett., 42* (1983) 597.
11 R. B. Schwarz and W. L. Johnson, *Phys. Rev. Lett., 51* (1983) 415.
12 F. R. de Boer, R. Boom, W. C. M. Mattens, A. R. Miedema and A. K. Niessen, in *Cohesion in Metals,* North-Holland, Amsterdam, 1988.
13 B. M. Clemens, R. B. Schwarz and W. L. Johnson, *J. Non-Cryst. Solids, 61&62* (1984) 817.
14 S. B. Newcomb and K. N. Tu, *Appl. Phys. Lett., 48* (1986) 1436.
15 J. C. Barbour, *Phys. Rev. Lett., 55* (1985) 2872.
16 J. B. Rubin and R. B. Schwarz, *Appl. Phys. Lett., 55* (1989) 36.
17 K. H. J. Buschow, *J. Phys. D: Appl. Phys., 14* (1981) 1087.
18 W. L. Johnson, *Prog. Mater. Sci., 30* (1986) 81.
19 R. B. Schwarz and P. Nash, *J. Met., 41* (1989) 27.
20 K. Kusonoki, K. Tsumuraya and S. Nishikawa, *Trans. Jpn. Inst. Met., 22* (1981) 501.
21 A. D. Le Claire, in N. L. Peterson and R. W. Siegel (eds.), *Properties of Atomic Defects in Metals,* North-Holland, Amsterdam, 1978, also published in *J. Nucl. Mater., 69&70* (1978) 70.
22 H. Ninomiya, M. Koiwa, Y. Minonishi and S. Ono, *Trans. Jpn. Inst. Met., 24* (1983) 665.
23 W. K. Warburton and D. Turnbull, in A. S. Nowick and J. J. Burton (eds.), *Diffusion in Solids: Recent Developments,* Academic Press, New York, 1975, p. 171.
24 H. Hahn and R. S. Averback, *Phys. Rev., B37* (1988) 6533.
25 H. Hahn, R. S. Averback and V. M. Shyu, in R. B. Schwarz and W. L. Johnson (eds.), *Solid State Amorphizing Transformation,* Elsevier, Lausanne, 1988, also published in *J. Less-Common Met., 140* (1988) 345.
26 R. B. Schwarz, J. B. Rubin and T. J. Tiainen, in H. Wiedersich and M. Meshii (eds.), *Science of Advanced Materials,* ASM International, Materials Park, OH, 1990, Chap. 1.
27 H. Schroeder, K. Samwer and U. Koster, *Phys. Rev. Lett., 54* (1985) 197.

28 A. M. Vredenberg, J. F. M. Westendorp, F. W. Saris, N. M. Van Den Pers and Th. H. de Keijser, *J. Mater. Res., 1* (1986) 774.
29 W. J. Meng, C. W. Nieh, E. Ma, B. Fultz and W. L. Johnson, *Mater. Sci. Eng., 97* (1988) 87.
30 K. Pampus, K. Samwer and J. Bottinger, *Europhys. Lett., 3* (1987) 581.
31 P. Ehrhart, R. S. Averback, H. Hahn, S. Yadavalli and C. P. Flynn, *J. Mater. Res., 3* (1988) 1276.
32 P. Nash and C. S. Jayanth, *Bull. Alloy Phase Diagrams, 5* (1984) 144.
33 Kaufmann and Bernstein, Computer calculation of phase diagrams, in J. L. Margrave (ed.), *Refractory Materials, A Series of Monographs,* Academic Press, New York, 1970, Vol. 4.
34 N. Saunders, CALPHAD, *9* (1985) 297.
35 N. Saunders and A. P. Miodownik, *J. Mater. Res., 1* (1986) 38.
36 R. J. Highmore, *Philos. Mag., B62* (1990) 455.
37 W. G. Burgers, *Physica, 1* (1934) 36.
38 H. I. Aaronson, H. B. Aaron and H. B. Kinsman, *Metallography, 4* (1971) 1.
39 A. C. Khachaturyan, *Theory of Structural Transformation in Solids,* Wiley, New York, 1983, p. 157.
40 W. L. Johnson, *Prog. Mater. Sci., 30* (1986) 81.
41 D. Turnbull, *Metall. Trans., 12* (1981) 217.
42 J. Dages, H. Gleiter and J. Perepezko, *Proc. Mater. Res. Soc. Symp., 57* (1987) 67.
43 J. H. Perepezko and J. S. Paik, *J. Non-Cryst. Solids, 61&62* (1984) 113.
44 H.-W. Kui and D. Turnbull, *J. Non-Cryst. Solids, 94* (1987) 67.
45 F. Simon, *Ann. Phys., 68* (1922) 278.
46 S. S. Chang and A. B. Bestul, *J. Chem. Phys., 56* (1972) 503.
47 W. Kauzmann, *Chem. Rev., 43* (1948) 219.
48 L. Pauling and R. C. Tollman, *J. Am. Chem. Soc., 47* (1925) 2148.
49 R. B. Schwarz and P. Nash, unpublished work, 1991.
50 A. L. Greer, *J. Less-Common Met., 140* (1988) 327.
51 H. J. Fecht, P. J. Desre and W. L. Johnson, *Philos. Mag., B59* (1989) 577.
52 R. B. Schwarz, P. Nash and D. Turnbull, *J. Mater. Res., 2* (1987) 456.
53 D. Turnbull, *J. Appl. Phys., 21* (1950) 1022.
54 F. Spaepen, *Acta Metall., 23* (1975) 729.
55 Z. Altounian, T. Guo-Hua and J. O. Strom-Olsen, *J. Appl. Phys., 54* (1983) 3111.
56 H. J. Fecht and W. L. Johnson, *Nature, 334* (1988) 6177.
57 H. J. Fecht and W. L. Johnson, *Mater. Sci. Eng., A133* (1991) 427.
58 W. L. Johnson, personal communication, 1992.